CHEMISTRY
A EUROPEAN JOURNAL

DOI: 10.1002/chem.200601137

Studies of a Cobalt(III) Complex of the MMP Inhibitor Marimastat: A Potential Hypoxia-Activated Prodrug**

Timothy W. Failes,[a] Carleen Cullinane,[b] Connie I. Diakos,[a] Natsuho Yamamoto,[a] J. Guy Lyons,[c] and Trevor W. Hambley*[a]

Abstract: We report a potential means of selectively delivering matrix metalloproteinase (MMP) inhibitors to target tumour sites by use of a bioreductively activated Co^{III} carrier system. The carrier, comprising a Co^{III} complex of the tripodal ligand tris(methylpyridyl)-amine (tpa), was investigated with the antimetastatic MMP inhibitor marimastat ($mmstH_2$). The X-ray crystal structure of $[Co(mmst)(tpa)]ClO_4 \cdot 4H_2O$ was determined and two-dimensional NMR revealed the existence of two isomeric forms of the complex in solution. Electrochemical analysis showed that the reduction potential of the complex is suitable for it to be bioreductively activated at hypoxic tumour sites. In vitro assays confirmed the stability of the prodrug in solution prior to reduction and revealed very low cytotoxicity against A2780 cells. In vivo testing in mice showed a higher level of tumour-growth inhibition by the complex than by free marimastat. Both free marimastat and and its Co^{III} complex increased metastasis in the model used, with the complex significantly more active.

Keywords: cobalt · drug delivery · hydroxamates · hypoxia · X-ray diffraction

Introduction

Over the last few decades, the focus of anticancer drug development has changed from agents that target non-specific intracellular processes such as DNA synthesis and replication, and nucleotide turnover. More recent understanding of tumour cell biology has led to the identification of cellular processes that are altered in cancer cells and are responsible for tumour growth and replication. Thus, new approaches to cancer therapy have involved the selective inhibition of enzymes involved in the process of tumour metastasis. The development of potent inhibitors of these enzymes has resulted in a new class of drugs that have antimetastatic and cytostatic action.[1]

One such therapy involves combating the action of specific matrix metalloproteinases (MMPs). MMPs are involved in connective-tissue breakdown, specifically, cleavage of matrix proteins into smaller fragments. MMPs are involved in essential tissue remodelling, such as occurs during embryonic development,[2] and in wound healing,[3] but they have also been implicated in disease states such as arthritis and tumour metastasis.[4] The catalytic domain of all MMPs consists of a Zn atom coordinated by three histidine residues, allowing two coordination sites for substrate binding in the activated form.[5] Variations in sequence and secondary structure give rise to the 30 currently known types of MMP that act on differing substrates and, hence, effect differing physiological outcomes.

Both the gene expression and the activation of MMPs are highly regulated in healthy cells, but they are overexpressed and/or activated in invasive tumour cells.[6–12] Overexpression of MMPs 2 and 9 (alternatively known as gelatinase A and B, respectively) has been shown to be highly correlated with the aggressiveness of tumours,[13,14] and furthermore, increased metastatic potential has been observed concomitantly with increased activity of MMP-9.[15,16] In general, levels of MMPs are elevated in cancer patients[17] and a high rate

[a] Dr. T. W. Failes, Dr. C. I. Diakos, N. Yamamoto, Prof. T. W. Hambley
Centre for Heavy Metals Research, School of Chemistry
University of Sydney, NSW 2006 (Australia)
Fax: (+61) 293-513-329
E-mail: t.hambley@chem.usyd.edu.au

[b] Dr. C. Cullinane
Developmental Therapeutics Unit
Peter MacCallum Cancer Institute
Melbourne, VIC 0800 (Australia)

[c] Dr. J. G. Lyons
Kanematsu Laboratories, Sydney Cancer Centre
Royal Prince Alfred Hospital, Camperdown NSW 2050 (Australia)

[**] MMP = matrix metalloproteinase

Supporting information for this article is available on the WWW under http://www.chemeurj.org/ or from the author.

of overproduction of MMPs correlates with poor prognosis.[18–20] This has led to considerable recent research in development of specific inhibitors of MMPs as an exciting new therapeutic approach, particularly in the prevention of tumour metastasis, the main cause of morbidity in cancer patients.[21] Most inhibitors are peptidomimetic molecules with a hydroxamate functional group that chelates to, and ultimately inactivates, the catalytic Zn atom.[22,23] Several of these inhibitors have progressed to clinical trials, for instance, batimastat, and the subsequently developed marimastat that reached phase III trials for a variety of cancer types.[24]

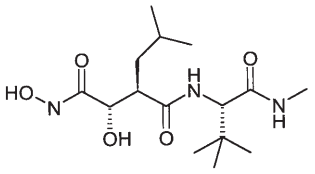

marimastat

Marimastat is a second-generation MMP inhibitor developed by British Biotech[25] as an orally available alternative to batimastat. The early pre-clinical studies established marimastat as a potent inhibitor of MMPs with some degree of selectivity, although it is generally regarded as a broad spectrum inhibitor. Testing against experimental metastasis models showed that marimastat administration reduced the number and size of metastatic foci in treated versus control animals.[24] Furthermore, these studies indicated a significant degree of cytostatic and tumour-growth-inhibitory activity. Marimastat progressed to phase III clinical trials, both alone and in combination with other chemotherapeutic agents, and is the first MMP inhibitor to be involved in randomised trials for cancer therapy.[26] The results of these trials are still under review, but indications suggest that marimastat does not produce sufficiently better results than existing therapies to warrant further development.

Whilst an incomplete understanding of the role of MMPs in tumour metastasis may explain the lack of efficacy of marimastat, it is also conceivable that inactivation of the hydroxamate group by metal ions in vivo may contribute. Hydroxamic acids have a strong affinity for many transition metals and there is considerable literature concerning the metal chemistry of hydroxamates.[27] In particular, hydroxamates bind strongly to Fe^{III} and, as such, have been used for many years in analytical chemistry as indicators of Fe^{III}.[28] In addition biologically active hydroxamates are important in Fe^{III} sequestration.[29–31] By contrast, little research has been applied to exploring the interaction of metal ions in vivo with MMP inhibitors, however we reported recently that there is some degree of inactivation of marimastat conferred by several transition metals in vitro.[32]

Our attention has been directed towards a means to "chaperone" MMP inhibitors to a site of action in an inactive form, whereupon the local chemical environment may be exploited to activate the drug. Inactivation of the inhibitor can be achieved in the same manner as we are trying to circumvent, by chelation to a metal ion. This in effect gives the metal ion a chaperoning role and there are some examples of this in the literature, most notably with copper non-steroidal anti-inflammatory drugs[33] and cytotoxic gold–phosphine complexes.[34] To achieve selective activation of a chaperone prodrug, we envisaged a bioreductively activated pathway, by exploiting the reductive environment of hypoxic tumours. This concept has been used by Ware and Denny and co-workers in developing Co^{III} complexes of nitrogen mustards as cytotoxic agents.[35,36] In principle, the Co^{III} complex provides an inert framework for transportation of the cytotoxic mustard, allowing cellular uptake and a cycle of reduction and back-oxidation. The hypoxic environment of tumour cells prevents this back-oxidation and the Co remains in the more labile +2 oxidation state, allowing release of the mustard in its active form. The method had moderate success at producing hypoxia selectivity, but the nature of the irreversibility of the reduction–oxidation cycle reduced the effectiveness of the prodrug.[37]

Accordingly, our aim was to extend this concept of a Co^{III} chaperone prodrug to MMP inhibitors. We report the synthesis of a Co^{III} complex of the MMP inhibitor marimastat with a tetradentate carrier ligand tris(methylpyridyl)amine (tpa). We have shown previously that Co^{III}tpa complexes with hydroximate ligands have reduction potentials consistent with hypoxia selectivity.[38] The complex was characterised in the solid state and in solution and we also report in vitro and in vivo studies of biological activity.

Results and Discussion

Synthesis: The synthesis of $[Co(mmst)tpa]ClO_4 \cdot 4H_2O$ ($mmstH_2$ = marimastat), **I**(ClO_4), proceeded smoothly and in good yield by displacement of the aqua and chloro ligands from $[CoCl(H_2O)tpa](ClO_4)_2 \cdot 3.5H_2O$ in aqueous media. Complex **I** was purified by ion-exchange chromatography and this enabled the formation of the Cl^- salt, **I**(Cl), used in the biological experiments.

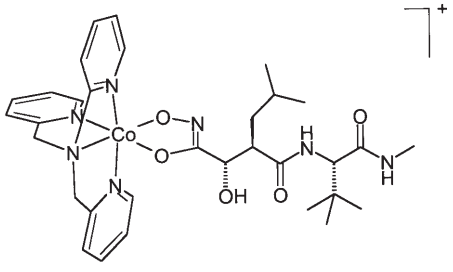

I

Crystallography: Single crystals of **I**(ClO_4) were grown from an aqueous solution of $NaClO_4$ and were analysed by X-ray diffraction. **I**(ClO_4) crystallises in the non-centrosymmetric

monoclinic space group $P2_1$. A thermal ellipsoid representation of the complex cation is given in Figure 1. The data-collection parameters and crystallographic parameters are listed in Table 1. Bond lengths and bond angles are listed in

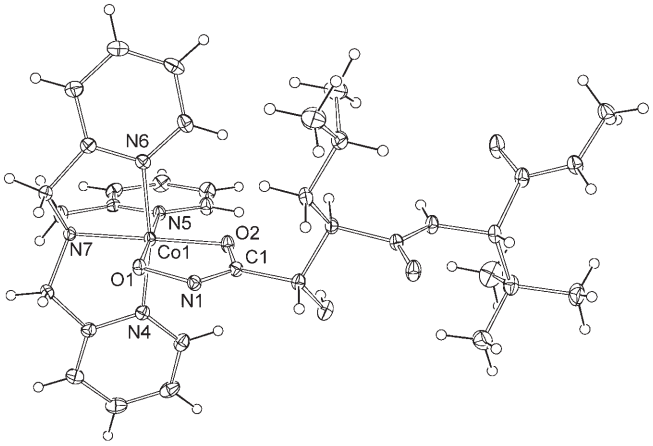

Figure 1. Thermal ellipsoid representation of the crystal structure of **I**-$(ClO_4)\cdot 4H_2O$. Perchlorate and water molecules are omitted for clarity, ellipsoids are shown at 30% probability. Crystallographic numbering of key atoms is given. Coordinate bond lengths Co(1)–O(1) 1.8693(12), Co(1)–O(2) 1.8693(13), Co(1)–N(4) 1.9304(15), Co(1)–N(5) 1.9332(14), Co(1)–N(6) 1.9273(13), Co(1)–N(7) 1.9444(15) Å.

the Supporting Information. Torsion angles, atomic coordinates and thermal parameters of the non-hydrogen atoms, as well as observed and calculated structural factors are available on request.

Table 1. Crystallographic and structural refinement data for **I**-$(ClO_4)\cdot 4H_2O$.

	I$(ClO_4)\cdot 4H_2O$
empirical formula	$C_{33}H_{53}ClCoN_7O_{13}$
formula weight	850.21
T [K]	150(2)
wavelength [Å]	0.71073
crystal system	monoclinic
space group	$P2_1$
a [Å]	8.5889(13)
b [Å]	18.950(3)
c [Å]	12.6315(19)
β [°]	97.277(3)
V [Å^3]	2039.4(5)
Z	2
ρ_{calcd} [Mg/m^3]	1.381
μ [mm^{-1}]	0.555
$F(000)$	892
$2\theta_{max}$ [°]	56.58
index ranges	$-11 \le h \le 11$, $-24 \le k \le 24$, $-16 \le l \le 16$
reflections collected	18214
independent reflections	9225 [R(int) = 0.0160]
refinement method	full-matrix least-squares on F^2
data/restraints/parameters	9225/2/538
goodness-of-fit on F^2	1.029
final R indices [$I > 2\sigma(I)$]	$R_1 = 0.0297$, $wR_2 = 0.0797$
R indices (all data)	$R_1 = 0.0309$, $wR_2 = 0.0804$
Flack parameter	0.015(7)
largest diff. peak and hole [e Å^{-3}]	0.798 and −0.603

The salt **I**(ClO_4) consists of a monovalent cationic species with a single perchlorate anion and four waters of crystallisation hydrogen bonded to the backbone of the marimastat ligand. The marimastat itself binds to the Co^{III} centre in an (O,O) fashion through the hydroxamate functionality in preference to other potential binding groups in the molecule. Coordination of the marimastat is in a manner such that the "hydroxyl" oxygen is *cis* to the tertiary amine nitrogen of the tpa tripod. The monovalent charge of the complex species with a single perchlorate anion indicates that the hydroxamate has adopted the doubly deprotonated hydroximate form in preference to the hydroxamate form. Analogous structures of simple hydroxamate complexes of the Co^{III}tpa system showed that both hydroxamato and hydroximato complexes may be obtained and interconverted by manipulation of pH.[38] However, only the hydroximate complex **I** could be obtained, despite efforts to obtain the hydroxamato form.

The coordination geometry of the Co^{III} centre is best described as pseudo-octahedral, with the best equatorial plane defined by the two oxygen-donor atoms, O(1) and O(2), of the marimastat and N(5) and N(7) of the tpa ligand with an average deviation of 0.01 Å. The structural parameters of the tpa ligand are consistent with previously described complexes and require no further discussion. The bond lengths from the oxygen donors O(1) and O(2) to the Co centre are in accord with other hydroximatocobalt(III) complexes;[39,40] 1.8693(12)and 1.8693(13) Å, respectively. Bond lengths of the hydroximate functionality are N(1)–O(1) 1.413(2), C(1)–N(1) 1.284(2), and C(1)–O(2) 1.331(2) Å which are similar to corresponding bond lengths in the reported hydroximato complexes.

The configuration of the ligand is such that the isopropyl arm is oriented toward one of the pyridyl arms of the tpa ligand. A number of close contacts are observed between hydrogen atoms of this pyridyl arm and those of the isopropyl group, with the shortest of these between H(7c) and H(29) at 2.98 Å. These types of interactions apparently dictate the overall conformation of the marimastat ligand. The remaining backbone is directed away from the Co centre with no evidence of any intramolecular interactions governing the position of the *tert*-butyl group. The bond lengths and angles of the marimastat are unexceptional. The peptide backbone adopts a conformation typical of a β-sheet structure in proteins; the dihedral angles ϕ and ψ, corresponding to the C–C′ and C–N bonds are 146.20(16) and −135.25(18)° respectively. The structure of free marimastat has not been reported and, therefore, this represents the first determination of the structure of this important compound.

NMR: An initial one-dimensional ^{1}H spectrum of **I**(ClO_4) was acquired in [D_7]DMF (Figure 2). The assignments were based on the observation of the intense peaks centred at approximately 0.4 and 0.9 ppm, which, based on the marimastat spectrum, are due to the methyl protons of the isopropyl and *tert*-butyl (*t*Bu) groups. Interestingly, both sets are

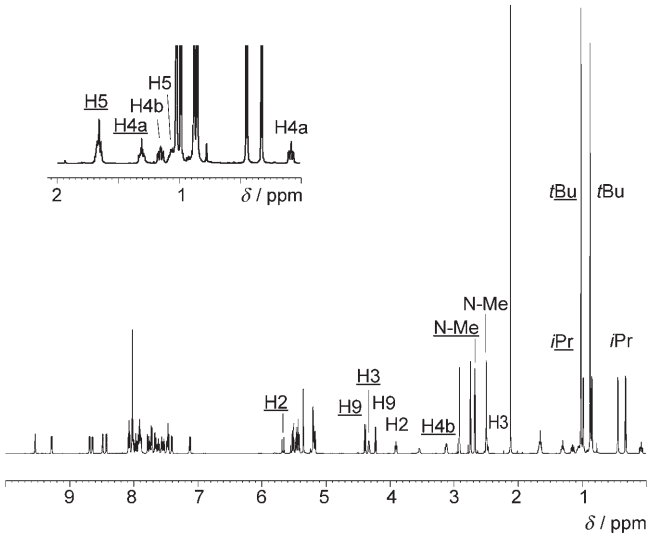

Figure 2. ^{1}H NMR spectrum of **I**(ClO_4) in [D_7]DMF.

split into "doublets" and furthermore, a second set of the isopropyl (*i*Pr) peaks appears centred slightly upfield of the *tert*-butyl resonances. The appearance of the "doublets" is likely to be the result of the magnetic inequivalence of the two methyl groups, which is enhanced by complexation of the marimastat. In this case, one methyl is directed toward the tpa ligand and the other away altering the relative chemical shifts. Observation of the second set of doublets, which both have the same intensity, is suggestive of isomerism in the complex, with the ratio of the two isomers close to 1:1. The isomerism arises because the hydroxyl oxygen of the coordinated marimastat may be either *cis* or *trans* to the tertiary amine nitrogen of the tpa ligand. The crystal structure revealed only the *cis* isomer, yet the *trans* may crystallise independently; because only a single band separated on the cation-exchange column, the two isomers may co-elute.

A two-dimensional COSY NMR spectrum was used to assign the remaining resonances of the marimastat ligand (Figure 3) and to elucidate the isomerism described above. The pyridyl ring protons were not assigned due to the clut-

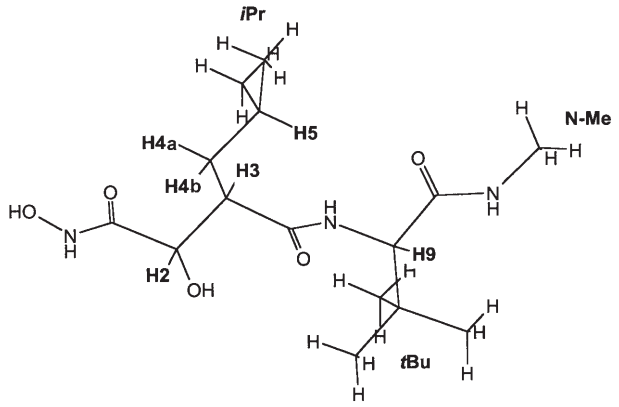

Figure 3. Main proton environments in marimastat.

tering of resonances in the aromatic region (7–8 ppm). Distinction between the *cis* and *trans* isomers was achieved by consideration of ring-current effects arising from the pyridyl rings of the tpa ligand. As shown in the diagrams of the *cis* and *trans* isomers (Figure 4), protons of the marimastat

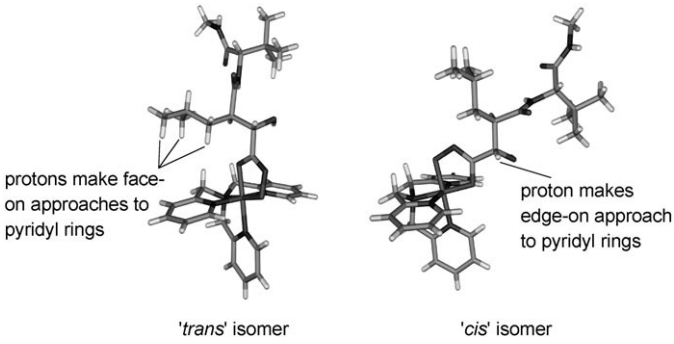

Figure 4. Illustration of the two isomers of **I**(ClO_4) and the interactions of marimastat protons with the pyridyl rings of the tpa ligand.

ligand may make approaches either coplanar or normal to the plane of these rings, leading to downfield or upfield shifts, respectively, of the corresponding resonances. An expansion of the COSY spectrum (Figure 5) highlights related cross-peaks for each isomer and shows the relative downfield shifting of resonances due to the *cis* isomer. A list of these resonances compared to the corresponding resonances

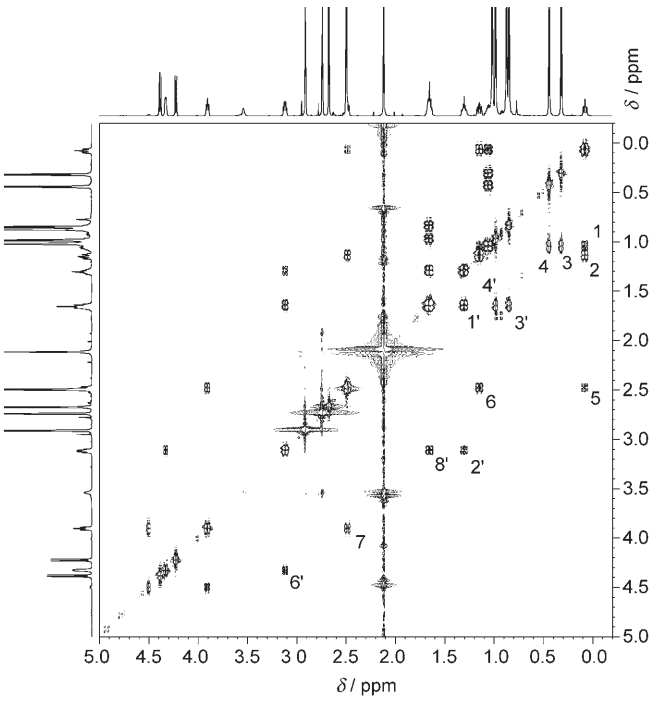

Figure 5. Expansion of region 0–5 ppm in the two-dimensional ^{1}H COSY spectrum of **I**(ClO_4). Major cross-peaks: 1 H4a/H5, 2 H4a/H4b, 3 and 4 *i*Pr/H5, 5 H3/H4a, 6 H3/H4b, 7 H2/H3, 8′ H4b/H5. Numbers with ′ correspond to cross-peaks of the *cis* isomer.

observed for free marimastat is given in Table 2. In general, the resonances in the *cis* isomer are shifted downfield, and for the *trans* upfield; this disparity is particularly apparent with the H4 and *i*Pr protons due to their proximity to the tpa ligand where the ring current effects would be expected to be most pronounced.

Table 2. ^{1}H NMR chemical-shift data for marimastat ligand protons in **I**-(ClO_4).[a]

Proton	Marimastat	*trans*-**I**(ClO_4)	*cis*-**I**(ClO_4)
H2	3.71	3.8	5.8
H3	2.69	2.49	4.3
H4	1.41	**a** 0.08 **b** 1.15	**a** 1.30 **b** 3.10
H5	0.95	1.1	1.65
H9	4.17	4.21	4.38
*i*Pr	0.89	0.32 0.44	0.84 0.98
*t*Bu	0.79	0.87	1.02
N-Me	2.56	2.50	2.68

[a] **a** and **b** can be found in Figure 3.

A NOESY spectrum was acquired to gain insight into the orientations of the ligands. In particular, it was hoped that cross-peaks between marimastat protons and pyridyl protons would be observed. As shown by the spectrum (Figure 6) the only cross-peaks observed were between resonances of marimastat protons that enabled confirmation of the assignments made previously. No cross-peaks were observed between resonances of the pyridyl region and the marimastat region. Cross-peaks of the *t*Bu groups correspond to correlation between *t*Bu protons and the amide proton to which they are adjacent. From the lack of such correlaton it can be presumed that either the interactions between marimastat and pyridyl protons were too weak to be observed, or there was some degree of rotation of the marimastat backbone around the C–C bond attaching it to the hydroxamate moiety. If this rotation were rapid relative to the timescale of the NMR experiment, then any cross-peaks would be weak and not readily observed.

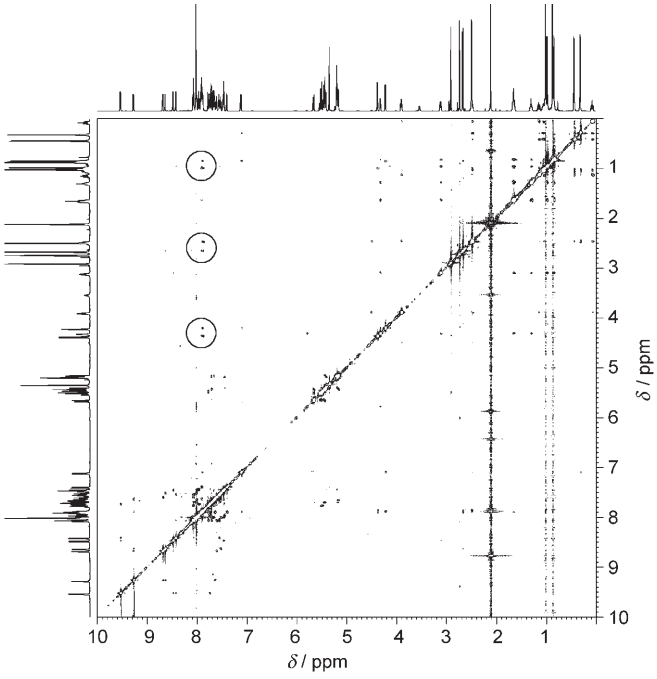

Figure 6. two-dimensional ^{1}H NOESY spectrum of **I**(ClO_4). Highlighted cross-peaks indicate coupling between *t*Bu and amide protons of the marimastat ligand.

Electrochemistry: Cyclic voltammetry (CV) was employed to determine the electrochemical characteristics of **I**(ClO_4), and a CV plot is given in Figure 7. At a scan rate of 500 mV s^{-1}, the observed reduction-oxidation wave is typical for an irreversible system with no anodic current detected upon scan reversal. Higher scan rates failed to resolve any degree of reversibility. This is typical for most Co^{III} complexes, as reduction to Co^{II} promotes total ligand substitution to form the hexa-aqua Co^{II} ion, $[Co(H_2O)_6]^{2+}$. Hence, the reduction potential is quoted as the cathodic peak potential E_{pc} and is listed in Table 3, along with values determined for the precursor complex and simple hydroxamate complexes of the Co–tpa system for comparison.

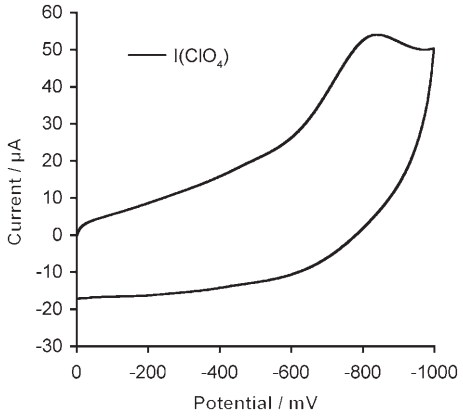

Figure 7. Cyclic voltammogram of **I**(ClO_4) in water at a scan rate of 500 mV s^{-1}.

The E_{pc} value for **I**(ClO_4) is quite low at −863 mV (vs. Ag/AgCl) and is slightly lower than the values determined for the simple hydroxamate complexes. On the other hand,

Table 3. Cathodic peak potentials (E_{pc}) for **I**(ClO_4) and other Co^{III}tpa complexes.

Complex	E_{pc} [mV] vs. Ag/AgCl
I(ClO_4)	−863
[Co(aha-H)tpa]ClO_4[a]	−834[38]
[Co(pha-H)tpa]ClO_4[b]	−789[38]
[Co(bha-H)tpa]ClO_4[c]	−770[38]
[CoCl(H_2O)tpa](ClO_4)$_2$	−166[38]

[a] aha = acetohydroxamic acid. [b] pha = phenylhydroxamic acid. [c] bha = benzohydroxamic acid.

the aqua chloro starting material has a relatively high reduction potential and, therefore, the hydroxamate functional group confers a greater degree of resistance to reduction than chloro and aqua ligands. The close grouping of E_{pc} values for all hydroxamate complexes suggests it is primarily the ligand donor atoms that control reduction potential, with hydroxamate substituents having only a modest influence. The question of whether these reduction potentials are appropriate for reduction of **I** in hypoxic conditions cannot be definitively assessed, as the study of redox properties of hypoxic tumours has not been adequately reported. Ware and Denny[36] suggested a target reduction potential of between −200 and −400 mV (vs. normal hydrogen electrode, NHE) to match that of cellular reductases, but clearly in our example, in which the prodrug is expected to act extracellularly, this is not necessarily appropriate.

Biological testing: An in vitro MMP inhibition assay was used to establish the base activity of **I**(Cl) in a non-reducing environment and, hence, its level of effectiveness as a chaperone for marimastat. The assay employed a standard fluorogenic substrate and IC_{50} values were calculated for the level of inhibition of MMP-9 by free marimastat and **I**(Cl) relative to a control sample. A list of these values is given in Table 4.

Table 4. IC_{50} values determined by the MMP inhibition assay

	IC_{50} [nM]
marimastat	7.0 ± 0.5
I(Cl)	900 ± 100

The IC_{50} value obtained for marimastat of 7.0 nM is reasonably close to the reported value of 3 nM, the disparity perhaps reflecting differing experimental conditions. A value of 900 nM was determined for the Co^{III} complex, more than two orders of magnitude greater than for the inhibitor alone. This difference is readily accounted for by the coordination of the hydroxamate moiety to the Co centre that renders it unable to bind to the catalytic Zn atom of the MMP. The measurable activity is likely to result from release of marimastat by aquation of the complex rather than the complex itself having any intrinsic inhibitory activity. An Fe^{III} complex of marimastat was found to have a higher level of activity, in line with Fe^{III} complexes being more labile than the relatively inert Co^{III}.[41] Thus, this result demonstrates that **I** is quite stable outside of a reducing environment and provides a suitable chaperone for marimastat, preventing it from being deactivated prior to reaching a tumour site.

The cytotoxicities of **I**(Cl) and the cobalt carrier complex $[CoCl_2(H_2O)(tpa)]ClO_4$ were determined by using the A2780 human ovarian cancer cell line. Both had very low toxicity: 172(18) and 77(6) μM respectively.

In vivo testing of **I**(Cl) for antimetastatic activity was used to assess the overall viability of the complex as a bioreductively activated prodrug. Administration of **I**(Cl) to Balb/c mice with 4T1.2 tumour implants was conducted over a 25 day period, and during that time the growth of the tumours was measured and compared to a control group and a group that had been administered free marimastat (Figure 8). The growth of the volume of the tumours appeared to be less for both the marimstat and the Co groups than for the control group, but by the end of the timecourse, only the Co group displayed a statistically significant difference. Pre-clinical studies reported marimastat to have some tumour-growth-inhibitory activity, but this is not reflected in this study. The observation of tumour-growth inhibition by the Co complex is interesting and, because both **I** and the carrier complex are non-cytotoxic, it is apparently the result of the complex being able to deliver marimastat more effectively. Reduction of **I** to the hexa-aqua Co^{II} ion, the likely reduced species as suggested by the electrochemical studies, would similarly be unlikely to exert a significant level of activity at this dosage level.

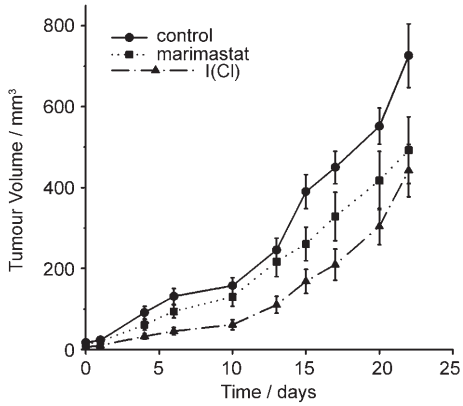

Figure 8. Growth of 4T1.2 tumours assessed as mean tumour volume for the three groups.

Upon completion of the experiment, the lungs, spine and femurs were harvested and the level of metastasis measured as tumour burden by using real time polymerase chain reaction (PCR). The results of these analyses are presented in Figure 9. Overall, the tumour levels in the target tissues of the control group were very low. Generally the tissues in this experimental model are harvested when the tumours reach around 1 g, with tumour levels being significant in both bone and the lungs. The failure of the primary tumours to reach this size may account for the low level of metastatic tumour burden observed in the control group.

The relative tumour burdens in both the marimastat and Co groups were higher than in the control group, with the difference in the lung being statistically significant. This result is unexpected, particularly for marimastat, which has been shown in similar in vitro metastasis models to exhibit potent metastatic inhibition.[24] An independent repetition of the PCR analysis for the lung samples was performed and as shown in Figure 9, was consistent with the earlier results. It should be noted that in previous studies of metastasis with

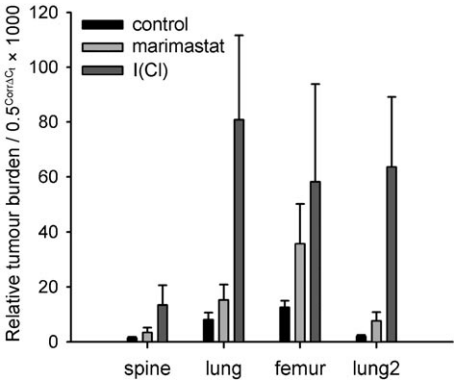

Figure 9. Metastatic potential for the three test groups. Lung2 represents a repeat analysis of the lung sample.

marimastat, the metastatic activity was assessed by counting metastases, whereas in this experiment, the activity was determined by performing a reproducible biochemical assay. Once again it is likely that the harvesting of the tumours prior to reaching a suitable size may account for the evident lack of inhibitory activity of marimastat. However, it is not clear why **I** would apparently potentiate metastasis — no evidence of other Co^{III} complexes nor free tpa having this effect exists in the literature.

Conclusion

This study demonstrates that MMP inhibitors can be deactivated by forming metal complexes and that this may be a useful means for protecting the hydroxamate moiety prior to reaching the tumour site. Furthermore, the Co–tpa ligand system examined provides the necessary structural and electrochemical framework for a bioreductively activated carrier. The crystal structure of **I** presented is the first structural characterisation of either marimastat or a metal complex thereof. We have shown that marimastat coordinates to the Co^{III} centre preferentially through the (*O,O*) donors of the hydroximate moiety, despite the presence of other chelating moieties. **I**(ClO_4) exists as *cis* and *trans* isomers in solution, as determined by two-dimensional NMR. The low reduction potential of **I**(ClO_4) indicates it has a strong likelihood of remaining intact prior to reaching a hypoxic site.

Although the preliminary biological testing provided seemingly contradictory results, it is interesting that the Co–marimastat complex displayed a higher level of tumour-growth inhibition than marimastat alone. Unexpectedly though, both marimastat and the cobalt complex gave rise to higher levels of metastatic potential than the control, which in the case of marimastat is inconsistent with studies showing it to have good anti-metastatic activity. The lack of sufficient tumour size was probably a factor in these results, and further experiments utilising a longer administration period are required to elucidate the effectiveness of the drugs.

Experimental Section

Marimastat ($mmstH_2$) was synthesised by Dr. Simone Vonwiller of the Organic Synthesis Centre, University of Sydney. The starting complex $[CoCl(H_2O)tpa](ClO_4)_2{\cdot}3.5\,H_2O$ was prepared by using a published procedure.[42] All other chemicals used were standard laboratory grade and were used as supplied.

Synthesis of $[Co(mmst)(tpa)]^+$ (I) complexes: Marimastat (90 mg, 0.27 mmol) was added to a stirred solution of $[CoCl(H_2O)tpa](ClO_4)_2{\cdot}3.5H_2O$ (0.18 g, 0.27 mmol) in water (2.5 mL) at 40 °C. The reaction mixture was neutralised with dropwise addition of aqueous NaOH (1 M). After stirring overnight to ensure complete reaction, the blue-green precipitate was filtered off, washed with a small amount of cold water and air-dried. The filtrate was loaded onto a cation-exchange column (Sephadex SP C-25, 0.5 × 5 cm) in the Na^+ form, the product was eluted with 0.1 M $NaClO_4$ and the blue-green band was collected. Upon slow evaporation of the eluant, green crystals of $[Co(mmst)tpa]ClO_4{\cdot}4\,H_2O$, **I**($ClO_4$), formed that were suitable for X-ray diffraction. Elemental analysis calcd (%) for $C_{33}ClH_{53}CoN_7O_{13}$ (850.2): C 46.62, H 6.28, N 11.53; found: C 46.38, H 6.09, N 11.21.

The chloride salt of this complex was prepared by substituting the 0.1 M $NaClO_4$ eluant with 0.1 M NaCl in the elution step and proceeding as described above. Elemental analysis of the complex gave erratic results, presumably due to the evaporation of water molecules in the crystal lattice. The X-ray crystal structure of this salt (data not shown) confirmed it to be the desired complex and to be of the same isomeric form as the perchlorate salt. All biological experiments were conducted with the Cl^- salt, **I**(Cl).

In both cases, attempts at forming the hydroxamato (mmstH) complex were made by titrating solutions with HCl (0.1 M); stable species could not be obtained and lowering the pH ultimately led to complete protonation of the ligand and rapid dissociation of the complex.

Single crystal X-ray crystallography: X-ray crystallographic analysis was performed on a suitable crystal of **I**(ClO_4) mounted on a thin glass fibre. All data were obtained at 150 K with a Bruker SMART 1000 CCD diffractometer using graphite monochromated Mo Kα radiation generated from a sealed tube. The low-temperature collection was performed by using an Oxford Systems Cryostream. An empirical absorption correction determined by using SADABS[43,44] was applied to the data. The data integration and reduction were undertaken by using SAINT and XPREP,[45] and subsequent computations were carried out by using the WinGX[46] graphical-user interface. The data reduction included the application of Lorentz and polarisation corrections. The structure was solved by direct methods using SHELXS-97 and was extended and refined with SHELXL-97.[47] The structures were refined on F^2 by using full-matrix least-squares with anisotropic thermal parameters for all non-H atoms and calculated (riding model) positions for H atoms, with U_{ij} set at 1.2 of that of the parent atom. Final *R* indices and weighting schemes are as quoted in the corresponding crystal-data tables. An ORTEP[48] representation of the structure was plotted with thermal ellipsoids at the 30% probability level (Figure 1).

Two-dimensional ^{1}H NMR: NMR experiments were performed on a Bruker Avance DMX 600 MHz spectrometer (University of New South Wales) equipped with a TXI triple-resonance probehead with triple axis gradients. Two-dimensional spectra were acquired in phase-sensitive mode with time-proportional phase incrementation. Spectra were acquired and processed by using Bruker XWinNMR software (version 2.6) on an SGI Indy workstation. Commercially available solvents (Aldrich or Merck) of at least 99.6% isotopic purity; all spectra were referenced to solvent isotopic impurities.

Experiments were performed by using standard Bruker pulse sequences (XWinNMR v2.6). One-dimensional ^{1}H spectra and two-dimensional DQF-COSY and NOESY results were acquired by means of water suppression by presaturation, over a spectral width of 8000 Hz. A DQF-COSY spectrum was collected with data sets resulting from 600 increments of t_1, with each free induction decay composed of 2048 data points. For each increment of t_1, 32 transients were recorded, with a recycle

delay of 1.8 sec used. A NOESY spectrum of mixing time (τ_m) 800 ms was acquired. Data sets resulting from 1024 increments of t_1 were recorded, with each free induction decay composed of 2048 data points. For each increment of t_1, 16 transients were recorded, with a recycle delay of 3 s. All spectra were processed by zero-filling and subjecting the data to shifted sine-bell weighting functions in F1 and F2 of $\pi/2$, and were baseline corrected by using Bruker XWinNMR software, version 2.6.

Electrochemistry: Electrochemical measurements were carried out by using a BAS 100B/W Electrochemical Analyzer system. A glassy carbon working electrode was used, the reference electrode was a BAS Ag/AgCl reference electrode filled with aqueous 3 M NaCl, and the auxiliary electrode was a platinum wire. Argon gas, which had previously been passed through an oxygen trap, was used to degas the aqueous solution of **I**(ClO_4) and supporting electrolyte $NaClO_4$ prior to measurements.

MMP inhibition assay by MDPF-labelled gelatin: The MMP-9 inhibitory activity of **I**(Cl) compared to that of free marimastat was determined by performing an in vitro proteolytic assay using a fluorogenated gelatin substrate. The protocol involved using four concentrations of **I**(Cl) within the appropriate concentration window plus a control sample of zero concentration in each assay, which was repeated three times for each complex.

Activated MMP-9 was prepared by using standard methods involving the reaction of proMMP-9 with aminophenylmercuric acetate (APMA) in Tris and Tris, $CaCl_2$, NaCl (TCN) buffers overnight at 37 °C followed by dialysis vs. TCN buffer (2 L) at 4 °C for 1 h. 40 μg of MDPF (2-methoxy-2,4-diphenyl-3(2H)-furanone)-labelled gelatin was incubated with **I**(Cl) and 0.05 μg of activated MMP-9 in TCN buffer overnight at 37 °C. Two control samples without MMP-9 were also prepared, in addition to a sample containing trypsin (12 μL) in order to establish the maximum level of substrate digestion.

Following incubation, the reaction was stopped with EDTA (60 μL, 20 mM), and ammonium sulfate (480 μL, 0.375 g mL^{-1}) was added to precipitate any undigested gelatin. Precipitation was not carried out for one of the control samples in order to establish the maximum fluorogenic activity. The samples were stored at 4 °C for 1 h and then centrifuged at 14000 rpm at 4 °C for 30 min. 500 μL of the solubilised products were measured by fluorescence spectrophotometry (370 nm excitation, 480 nm emission) and the IC_{50} values were determined as the drug concentration that reduced the absorbance to 50% of the untreated control sample.

In vivo metastasis testing

By using an experimental metastasis model, the in vivo activity of **I**(Cl) was compared to that of free marimastat in mice. The experimental protocol was codesigned and carried out by Dr. Carleen Cullinane at the Peter MacCallum Cancer Institute, Melbourne.

Cell culture: 4T1.2 tumour cells were grown in standard tissue-culture plasticware in a 5% CO_2 atmosphere incubator in αMEM (minimal essential medium) containing 10% foetal calf serum (FCS) and antibiotics. In preparation for injection, cells were removed from culture dishes by adding 0.02% EDTA in phosphate buffered saline (PBS), washing once with PBS and then resuspending in PBS at the appropriate concentration.

Mouse injections: A 10 μL aliquot of cells (1×10^7 cells mL^{-1}) was mixed with 10 μL of matrigel that had been thawed on ice. The 20 μL cell/matrigel mix was then injected into the fourth mammary fat pad of ten-week-old female Balb/c mice. Mice were briefly sedated with penthrane during this procedure. Tumours became palpable within seven days. To ensure maximum metastatic growth, 4T1.2 tumours were grown for 28 days prior to drug administration. Selected mice with comparable tumour size were randomised into three groups — a control group and separate groups to be treated with each drug. The dosage of the drugs was 10 mg kg^{-1} d^{-1} for marimastat and 21.5 mg kg^{-1} d^{-1} for **I**(Cl) injected once daily in a saline solution. Drug administration continued for 22 days with the tumour volume measured during this time period. Upon completion of the experiment the mice were euthanased and the tumours were excised and weighed. The lungs, femurs and spines were harvested and then frozen in liquid N_2. The tissues were pulverised in steel homogenisers (cooled with liquid N_2) to produce a fine powder. Amounts of approximately 50 mg were digested with proteinase and the DNA was extracted by using routine methods.

Real-time quantitative PCR (RTQ-PCR): This assay is based on the ability of RTQ-PCR to measure the number of copies of the neomycin resistant gene (neo^r), present only in the transfected tumour cells, relative to that of an endogenous gene that is present in all cells. Primers and fluorescent probes to neo^r and vimentin were designed by using the Primer Express software to utilise the TaqMan 5′ fluorogenic-assay method. Testing, optimisation and assays were all performed by using either an ABI Prism7700 or an ABI Prism7000.

Relative-tumour-burden calculations: Relative-tumour-burden (RTB) calculations were based on the comparative Ct method by using a multiplex reaction. For each sample, the threshold cycle (C_t) value of the vimentin amplification profile was subtracted from the C_t value of the amplification profile to provide the ΔC_t value. The ΔC_t value represents the difference in the number of PCR cycles required for the two amplicons to reach a specified threshold. A corrected ΔC_t value ($Corr\Delta C_t$) for each group was calculated to account for the different copy number of neo^r in each cell line. Each cycle represents a two-fold difference in the abundance of the target sequence, therefore, RTB can then be calculated using the following formula:

$$RTB = {}^1/_2{}^{Corr\Delta C_t} \times 10000$$

A multiplication factor of 10000 was applied to this equation to produce a final RTB value that generally falls within the range of 0–10000. The RTB for each treatment group was then calculated by taking the average of individual RTB values. Standard errors of the mean (SEM) and p-values were calculated using the standard T-test.

Cytotoxicity assay: Human ovarian carcinoma cell lines A2780 were maintained in exponential growth as monolayers in Advanced DMEM supplemented with 2.5 mM glutamine and 2% fetal calf serum at 37 °C in 5% CO_2. Complexes tested were prepared as 1 and 5-mM aqueous solutions containing 5% DMF immediately prior to the assay. Cytotoxicity was determined by using the 3-(4,5-dimethylthiazol-2-yl)-2,5-diphenyltetrazolium bromide (MTT) assay as previously described.[49] Single cell suspensions were obtained by trypsinisation of monolayer cultures, and cell counts were performed by using a haemocytometer counter (Weber). Approximately 1×10^5 cells in 100 μL culture medium were seeded onto each well of flat-bottomed 96-well plates (Becton Dickinson) and allowed to attach overnight. Cobalt-complex solutions were diluted in culture medium such that 5-40 μL of each drug solution added to quadruplicate wells produced the final desired concentrations spanning a 4-log range (final DMF concentrations were limited to 0.5%). Following incubation of the cells for 72 h, MTT (1.0 mM) was added to each well incubation continued for a further 4 h. The culture medium was then removed from each well and DMSO (150 μL) (Sigma) was added, the plate was shaken for 5 s and the absorbance was measured immediately at 600 nm by using a Victor^{3}V microplate reader (Perkin–Elmer). IC_{50} values were determined to be the drug concentration that reduced the absorbance to 50% of that in untreated control wells.

Acknowledgements

We wish to thank the Sydney University Cancer Research Fund for financial support.

[1] B. R. Zetter, *Ann. Rev. Med.* **1998**, *49*, 407–424.
[2] S. J. Fisher, C. H. Damsky, *Semin. Cell Biol.* **1993**, *4*, 183–188.
[3] U. K. Saarialho-Kere, A. P. Pentland, H. Birkedal-Hansen, W. C. Parks, H. G. Welgus, *J. Clin. Invest.* **1994**, *94*, 79–88.
[4] N. Johansson, M. Ahonen, V.-M. Kahari, *Cell. Mol. Life Sci.* **2000**, *57*, 5–15.
[5] W. Bode, C. Fernandez-Catalan, H. Tschesche, F. Grams, H. Nagase, K. Maskos, *Cell. Mol. Life Sci.* **1999**, *55*, 639–652.

[6] B. Davidson, I. Goldberg, P. Liokumovich, J. Kopolovic, W. H. Gotlieb, L. Lerner-Geva, I. Reder, G. Ben-Baruch, R. Reich, *Int. J. Gynecol. Pathol.* **1998**, *17*, 295–301.
[7] S. R. Bramhall, *Int. J. Pancreatol.* **1997**, *21*, 1–12.
[8] J. van 't Veer Laura, H. Dai, J. van de Vijver Marc, D. He Yudong, A. M. Hart Augustinus, M. Mao, L. Peterse Hans, K. van der Kooy, J. Marton Matthew, T. Witteveen Anke, J. Schreiber George, M. Kerkhoven Ron, C. Roberts, S. Linsley Peter, R. Bernards, H. Friend Stephen, *Nature* **2002**, *415*, 530–536.
[9] B. Nawrocki, M. Polette, V. Marchand, M. Monteau, P. Gillery, J.-M. Tournier, P. Birembaut, *Int. J. Cancer* **1997**, *72*, 556–564.
[10] A. Lochter, M. J. Bissell, *Apmis* **1999**, *107*, 128–136.
[11] A. Kugler, B. Hemmerlein, P. Thelen, M. Kallerhoff, H. J. Radzun, R. H. Ringert, *J. Urol.* **1998**, *160*, 1914–1918.
[12] H. Sato, T. Takino, Y. Okada, J. Cao, A. Shinagawa, E. Yamamoto, M. Selki, *Nature* **1994**, *370*, 61–65.
[13] E. C. Kohn, L. A. Liotta, *Cancer Res.* **1995**, *55*, 1856–1862.
[14] J. M. Ray, W. G. Stetler-Stevenson, *Embo J.* **1995**, *14*, 908–917.
[15] J. Hua, R. J. Muschel, *Cancer Res.* **1996**, *56*, 5279–5284.
[16] E. J. Bernhard, S. B. Gruber, R. J. Muschel, *Proc. Natl. Acad. Sci. USA* **1994**, *91*, 4293–4297.
[17] S. Zucker, M. Hymowitz, C. Conner, H. M. Zarrabi, A. N. Hurewitz, L. Matrisian, D. Boyd, G. Nicolson, S. Montana, *Ann. N. Y. Acad. Sci.* **1999**, *878*, 212–227.
[18] G. I. Murray, M. E. Duncan, P. O'Neil, J. A. McKay, W. T. Melvin, J. E. Fothergill, *J. Pathol.* **1998**, *185*, 256–261.
[19] G. I. Murray, M. E. Duncan, P. O'Neil, W. T. Melvin, J. E. Fothergill, *Nat. Med.* **1996**, *2*, 461–462.
[20] H. Yamamoto, Y. Adachi, F. Itoh, S. Iku, K. Matsuno, M. Kusano, Y. Arimura, T. Endo, Y. Hinoda, M. Hosokawa, K. Imai, *Cancer Res.* **1999**, *59*, 3313–3316.
[21] M. R. Alison, C. E. Sarraf, *Understanding Cancer: From Basic Science to Clinical Practice*, Cambridge University Press, Cambridge, **1997**.
[22] M. Whittaker, C. D. Floyd, P. Brown, A. J. H. Gearing, *Chem. Rev.* **1999**, *99*, 2735–2776.
[23] M. R. Michaelides, M. L. Curtin, *Curr. Pharm. Des.* **1999**, *5*, 787–819.
[24] M. Hidalgo, S. G. Eckhardt, *J. Natl. Cancer Inst.* **2001**, *93*, 178–193.
[25] J. P. Dickens, M. J. Crimmin, R. P. Beckett, (British Bio-Technology Limited, UK), PCT Int. Appl. WO 9005719, **1994**.
[26] S. R. Bramhall, A. Rosemurgy, P. D. Brown, C. Bowry, J. A. C. Buckels, L. Lambiase, A. Langleben, M. Shparber, J. Clark, P. Kaywin, J. Lutzsky, P. Benedetto, P. Boasberg, H. Harris, G. Leichman, D. Casciato, J. Harris, S. Mani, D. Van Echo, S. Dutta, B. Culliney, S. Zaknoen, A. Cohn, P. Byrne, D. Waterhouse, D. Brookes, H. Garewel, A. Staddon, B. Cynwyd, L. Einhorn, R. Winston, I. Berkowitz, A. Keller, G. Goldsmith, C. Imrie, C. Johnson, F. Daniel, H. Scarffe, M. Spittle, R. Charnley, H. Barr, D. Lloyd, W. Steward, J. Neoptolemos, S. Falk, T. Wheeler, D. Cunningham, P. Guillou, S. Van Belle, J. Moreau, M. Delgado, R. Houston, S. Rosewicz, P. Malfertheiner, M. Buchler, *J. Clin. Oncol.* **2001**, *19*, 3447–3455.
[27] B. Kurzak, H. Kozlowski, E. Farkas, *Coord. Chem. Rev.* **1992**, *114*, 169–200.
[28] J. W. Munson, *Chem. Biol. Hydroxamic Acids, [Proc. Int. Symp.], 1 st* **1982**, 1–13.
[29] J. R. Telford, K. N. Raymond, in *Comprehensive Supramolecular Chemistry, Vol. 1*, Elsevier, Oxford, **1996**, pp. 245–266.
[30] K. N. Raymond, G. Muller, B. F. Matzanke, *Top. Curr. Chem.* **1984**, *123*, 49–102.
[31] P. J. Giardina, R. W. Grady, *Semin. Hematol.* **2001**, *38*, 360–366.
[32] C. K. Underwood, D. Min, J. G. Lyons, T. W. Hambley, *J. Inorg. Biochem.* **2003**, *95*, 165–170.
[33] J. E. Weder, C. T. Dillon, T. W. Hambley, B. J. Kennedy, P. A. Lay, J. R. Biffin, H. L. Regtop, N. M. Davies, *Coord. Chem. Rev.* **2002**, *232*, 95–126.
[34] S. J. Berners-Price, C. K. Mirabelli, R. K. Johnson, M. R. Mattern, F. L. McCabe, L. F. Faucette, C. M. Sung, S. M. Mong, P. J. Sadler, S. T. Crooke, *Cancer Res.* **1986**, *46*, 5486–5493.
[35] D. C. Ware, W. R. Wilson, W. A. Denny, C. E. F. Richard, *J. Chem. Soc. Chem. Commun.* **1991**, 1171–1173.
[36] D. C. Ware, B. D. Palmer, W. R. Wilson, W. A. Denny, *J. Med. Chem.* **1993**, *36*, 1839–1846.
[37] D. C. Ware, H. R. Palmer, F. B. Bruijn, R. F. Anderson, P. J. Brothers, W. A. Denny, W. R. Wilson, *Anti-Cancer Drug Des.* **1998**, *13*, 81–103.
[38] T. W. Failes, T. W. Hambley, *Dalton Trans.* **2006**, 1895–1901.
[39] K. Abu-Dari, S. J. Barclay, P. E. Riley, K. N. Raymond, *Inorg. Chem.* **1983**, *22*, 3085–3089.
[40] A. Bino, *J. Am. Chem. Soc.* **1987**, *109*, 275–276.
[41] T. W. Failes, T. W. Hambley, *J. Inorg. Biochem.*, in press.
[42] J. B. Mandel, C. Maricondi, B. E. Douglas, *Inorg. Chem.* **1988**, *27*, 2990–2996.
[43] R. H. Blessing, *Acta Crystallogr. Sect. A* **1995**, *51*, 33-37.
[44] G. M. Sheldrick, SADABS: Empirical Absorption Correction Program for Area Detector Data, University of Göttingen, Göttingen (Germany), **1996**.
[45] Bruker Analytical X-ray Instruments Inc., SMART, SAINT and XPREP: Area Detector Control and Data Integration and Reduction Software, Madison, Wisconsin (USA), **1995**.
[46] L. J. Farrugia, *J. Appl. Crystallogr.* **1999**, *32*, 837-838.
[47] G. M. Sheldrick, SHELX97: Programs for Crystal Structure Analysis (Release 97-2), University of Göttingen, Göttingen (Germany), **1998**.
[48] C. K. Johnson, *ORTEPII*, *Report ORNL-5138*, Oak Ridge National Laboratory, Oak Ridge, Tennessee, **1976**.
[49] J. Carmichael, W. G. DeGraff, A. F. Gazdar, J. D. Minna, J. B. Mitchell, *Cancer Res.* **1987**, *47*, 943–946.

Received: August 7, 2006
Published online: December 15, 2006

